Search for NMSSM Higgs $h \to aa \to \mu\mu\mu\mu$

(Dated: April 9, 2009)

We present a study ...

PACS numbers: 13.38.Dg 13.38.Qk

I. INTRODUCTION

Tension between the electroweak data fits preferance for light higgs and limits from direct searches can be resolved by an elegant solution handed by the NMSSM. A possible solution could be that there is a new mode for higgs decay $h \to aa$, where a is a pseudoscalar higgs field, thus diminishing the branching ratios for conventional modes used in direct higgs searches and largely softening direct higgs mass limits from LEP. While 'naturalness' and 'fine tuning' arguments have lead to somewhat extensive studies of the region of masses of a above $\tau\tau$ and $b\bar{b}$ threshold, the results require a substantial integrated luminosity and are technically very challenging analysis.

At the same time, the region of lower masses (below $2m_\tau$) has not been studied. We propose here an analysis targeting the range of m_a below the $\tau\tau$ threshold by exploring the decay $h \to aa\mu\mu\mu\mu$. Unlike searches with taus, the two muon mass gives a direct estimate of m_a providing a substantially better constrained system. Further, this channel is essentially free of backgrounds and therefore one can use direct gluon fusion production instead of smaller vector boson fusion process that has to be used in order to suppress large QCD backgrounds.

Current constraints in this region come from XXX and are fairly weak - need SASHA's help here.

We show that the analysis in the four muon mode has excellent sensitivity for higgs and can be performed with just a handful of first CMS data and requires very little in terms of detector performance except reasonably robust tracking for muons and well functioning muon system. To make this a realistic analysis, we use parameters of the CMS experiment in designing selections and estimating background contributions.

II. NMSSM PARAMETER SPACE

The allowed NMSSM parameter space permits at least two phenomenologically-distinct Higgs systems, one in which a 120 GeV scalar Higgs decays primarily into conventional WW^*, $b\bar{b}$, and $\tau^+\tau^-$ modes, and another with a light, hidden Higgs that decays almost exclusively into aa. The latter has only been excluded up to 86 GeV by specialized searches at LEP (upper limit due to $e^+e^- \to hZ$ kinematics) [23, 24], leaving the 86–120 GeV region unexplored (Fig 1).

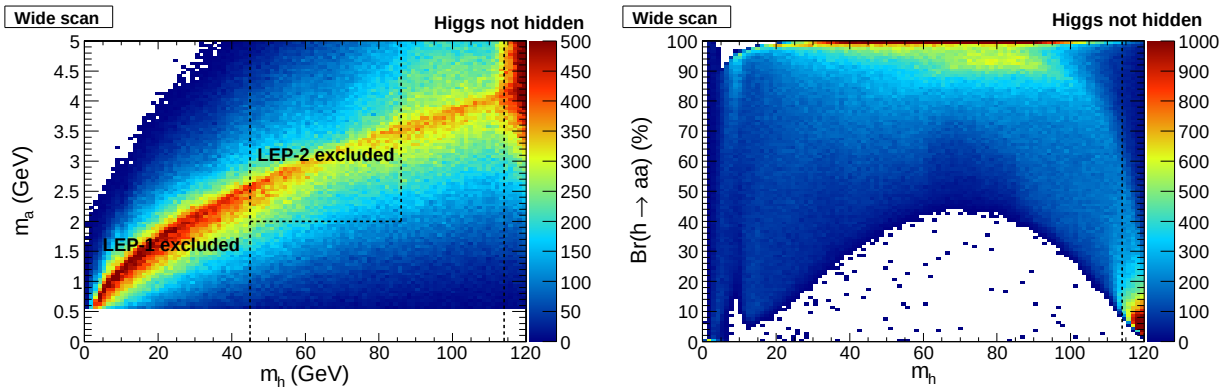

FIG. 1: Left: regions of m_a vs. m_h excluded by LEP searches, right: the strong correlation between m_h and $B_{h\to aa}$. The above scan is subject to experimental constraints (other than the two specialized LEP searches for $h \to aa$) which require a conventionally-decaying Higgs to have $m_h > 114$ GeV.

We used the NMSSMTools package [25–27] to scan the NMSSM parameter space and to identify the region with $B_{h\to aa} \gg B_{h\to WW^*,\, b\bar{b},\, \tau^+\tau^-}$. Scans are uniform in each parameter listed in Table I, subject to phenomenological and experimental constraints except for the specialized LEP $h \to aa$ searches. Two scans were performed, labeled "wide" and "narrow," where the narrow scan focuses more exclusively on the hidden Higgs region. The λ and A_κ parameters are restricted even in the wide scan to yield small m_a values, important for large $B_{a\to\mu\mu}$. A particularly important

parameter for distinguishing between conventional Higgs decays and hidden decays is the ratio of κ over λ, so we perform uniform scans in this ratio, rather than κ alone. Fig 3 shows how each parameter is related to $B_{h\to aa}$.

TABLE I: Ranges for NMSSM parameter scans. The narrow scan focuses on the region with high $B_{h\to aa}$.

Wide scan	Narrow scan
$0 < \kappa/\lambda < 0.8$	$0 < \kappa/\lambda < 0.5$
$0 < \lambda < 0.1$	*same*
$-0.1 < A_\kappa < 0$ GeV	*same*
$0 < A_\lambda < 4$ TeV	$1 < A_\lambda < 3$ TeV
$100 < \mu < 200$ GeV	$100 < \mu < 150$ GeV
$10 < \tan\beta < 60$	$10 < \tan\beta < 33$

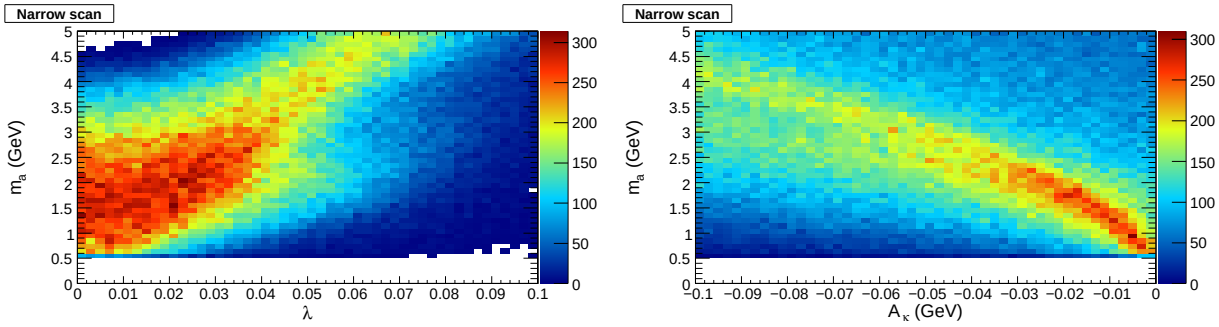

FIG. 2: Both λ and A_κ must be close to zero for m_a to be below the $2\,m_\tau$ threshold.

To determine the sensitivity of our 4-muon search channel, we also need to know the branching fraction of $a\to\mu\mu$. In the mass range of interest (below the $a\to\tau^+\tau^-$ threshold), the main competing channels are $a\to gg$ and $a\to s\bar{s}$. We again use NMSSMTools to calculate these (with $m_s = 95$ MeV and no cut on m_a), which are nearly a function of m_a only. The final branching fractions are presented in Fig 4.

A. Production Cross Section $pp\to h + X$

Due to relatively low expected backgrounds in the case of the four muon channel, one should go after the dominant production modes of higgs boson. We include $gg\to h$ and $bb\to h$. The higgs production cross-section is calculated in the framework of NMSSM for typical sets of parameters using XXX and YYY. Figure 2 shows the predicted cross-section for several typical choices of parameters and also a comparison with the Standard Model higgs production cross-section. **Need Sasha to write this one!!!**

III. ANALYSIS

The main characteristic of the signal is two back-to-back di-muon pairs with pair consisting of spatially close muons. The di-muon pairs should have invariant masses consistent with each, which serve as a measurement of m_a, and the four muon invariant mass distributionshould have a spike that corresponding to the m_h mass. We use these striking features of signal events in designing the analysis with a reasonably high acceptance and very low backgrounds suitable for early LHC running.

A. Signal Simulation

We use Pythia to generate signal event templates with m_h in the range from 70 to 140 GeV/c^2 and m_a in the range from 0.5 to 4 GeV/c^2). For detector response emulation, we chose the CMS detector as a benchmark and

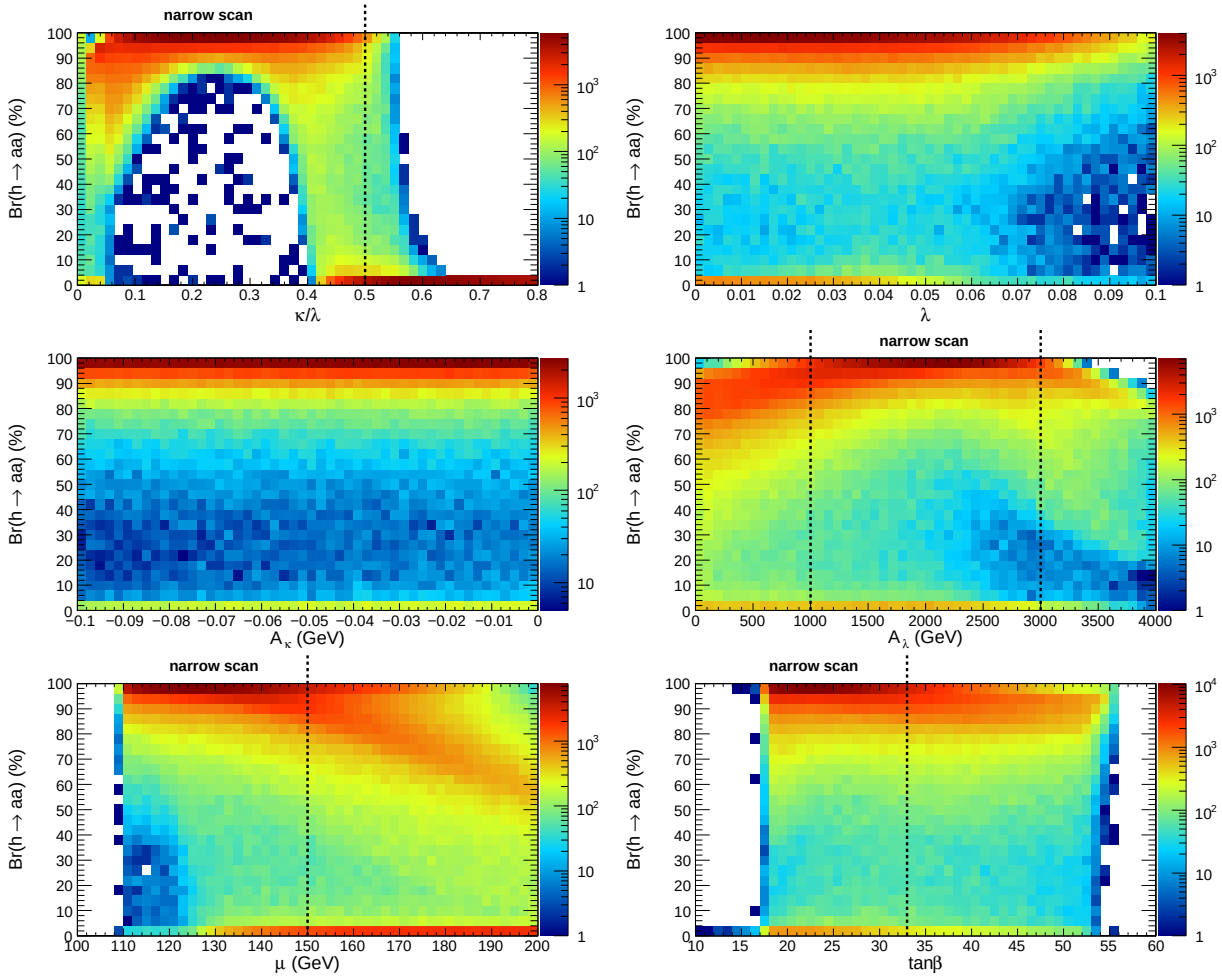

FIG. 3: $B_{h\to aa}$ as a function of each of the NMSSM parameters with dashed lines indicating the "narrow scan" cuts (Table I). All narrow scan cuts are applied except for the one shown. Note the logarithmic color scale used to highlight the difference between $B_{h\to aa} \approx 0\%$ and $\approx 100\%$.

used its parameters descibed in CMS Technical Design Report. The key parameters important for this analysis are muon momentum resolution, low threshold on muons to reach the muon system, acceptance and average muon reconstruction efficiencies. **we should quote the numbers.**

B. Event Reconstruction

The analysis starts by requiring at least four muon candidates with $p_T > 5$ GeV/$c$in the fiducial volume of the detector. At least one of the four muons has to have $p_T > 20$ GeV/c to suppress major backgrounds and to satisfy trigger requirements. Each event must have at least two muon candidates of positive and negative charge each. In events satisfying these critiria, we define quadruplets of candidates consisting of two positive and two negatively charged muon candidates. Although very unlikely, there can be more than one quadruplet per event, e.g. if there are five muons in the event. Each such quadruplet if preserved until the end of the analysis.

Next, we sort the four muon candidates in quadruplet into two di-muon pairs. We minimize the quantity $(\Delta R(\mu_i,\mu_j)^2 + \Delta R(\mu_k,\mu_l)^2)$ under the constarint that each di-muon pair consists of two muon candidates of opposite charge. We discard quadruplets in which ΔR between muons in any of the two pair exceeds **0.5???** as this cut is 100% efficient for the signal while it can diminish the size of the data sample by removing events, which have topology inconsistent with signal. At his point in the analysis, the invariant mass of each of the di-muon pair, $m_{12} and m_{34}$, is calculated as well as the invariant mass of all four muons, which we denote as m_{1234} or M. Figure 5a) shows the invariant mass of the muon pairs passing all selections (m_{12} and m_{34} are combined into a single distribution) for two

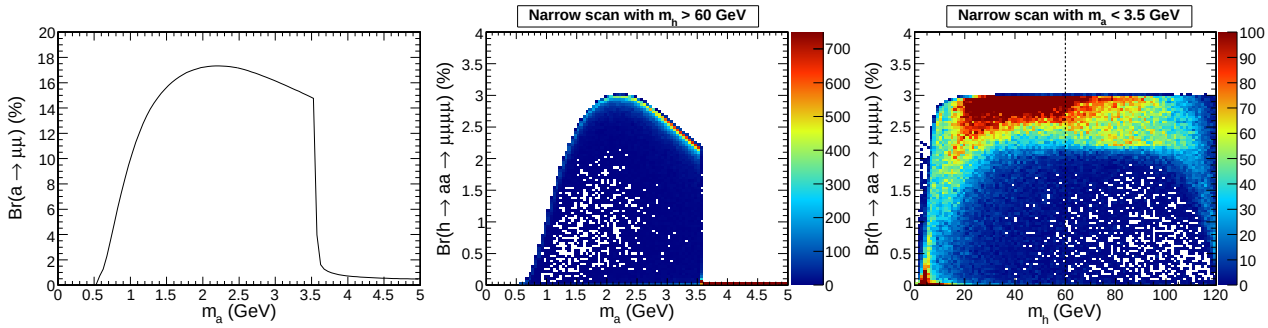

FIG. 4: Branching fractions of $a \to \mu\mu$ and full $h \to aa \to \mu\mu\mu\mu$ chain as a function of m_a and m_h.

TABLE II: Acceptances for various points in m_h-m_a space.

m_h, m_a (GeV)	0.5	1.0	2.0	3.0	4.0
80	0.3052 ± 0.0046	0.2656 ± 0.0044	0.2420 ± 0.0043	0.2389 ± 0.0043	0.2324 ± 0.0043
100	0.3915 ± 0.0049	0.3245 ± 0.0047	0.2906 ± 0.0045	0.2862 ± 0.0045	0.2819 ± 0.0045
120	0.4587 ± 0.0050	0.3785 ± 0.0049	0.3405 ± 0.0047	0.3226 ± 0.0047	0.3103 ± 0.0046

choices of m_h and m_a. Figure 5b) shows the distribution of the invariant mass M of the four muon system for two benchmark points. Further background suppression can be obtained by adding the isolation requirement to one or both di-muon pairs in the event, e.g. by setting the upper bound on the sum of transverse momenta of all tracks in a cone around the reconstructed direction of the di-muon pair excluding momenta of the two muon tracks. Such requirement can allow a very substantial suppression of the dominant source of the background coming from events with one or more muons originating from jets. We choose not to use this critirea as our estimates show that the final rate of such background events is already very low. If data shows larger contribution of these events, this isolation requirement would allow bringing backgrounds back to very low level at a moderate cost to signal acceptance.

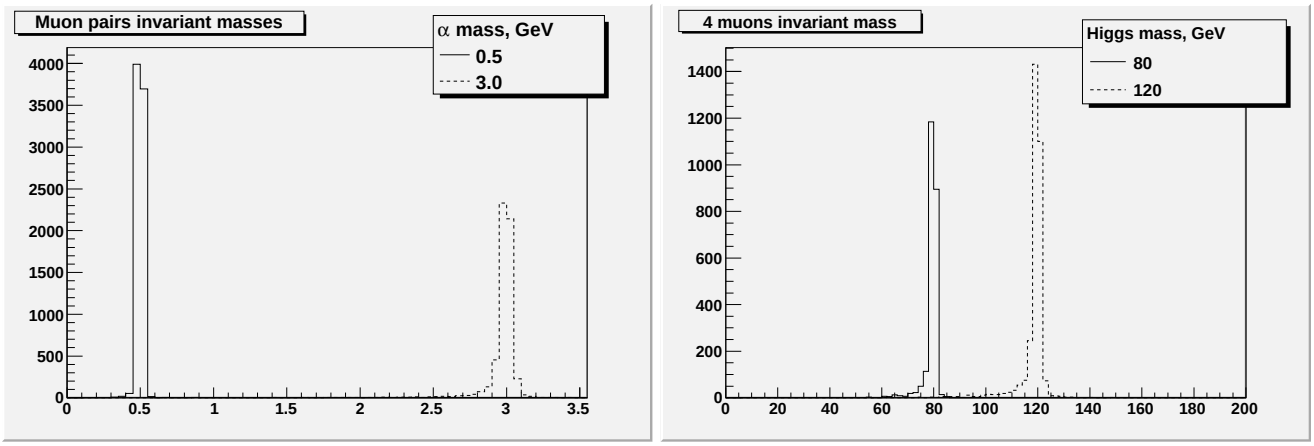

FIG. 5: Left: Reconstructed invariant mass of reconstructed muon pairs for $m_a = 0.5$ and 3 GeV/c^2 (in both cases $m_H = 100$ GeV/c^2). Right: Reconstructed invariant of four muons for $m_H = 80$ and $m_H = 120$ GeV/c^2 (in both cases $m_a = 3.0$ GeV).

Acceptance of the selections listed above is shown in Table II and is large thanks to the high coverage of the CMS muon system. Figures 6a) and 6b) illustrate the dependence of acceptance on values of m_h and m_a.

One can further reduce the background events and zoom on the region of interest of this analysis by applying cuts on m_{12}, m_{34}, M, and require that measured values of m_{12} and m_{34} are consistent within uncertainties. Instead of applying these cuts explicitly, we develop a statistical procedure that performs a fit in a 3D space of measured values of $(m_{12}, m_{34}, m_{1234})$ taking into account kinematical properties of signal events. This approach allows maximizing signal acceptance and therefore statistical power of the analysis and is discussed in what follows. It is also convenient

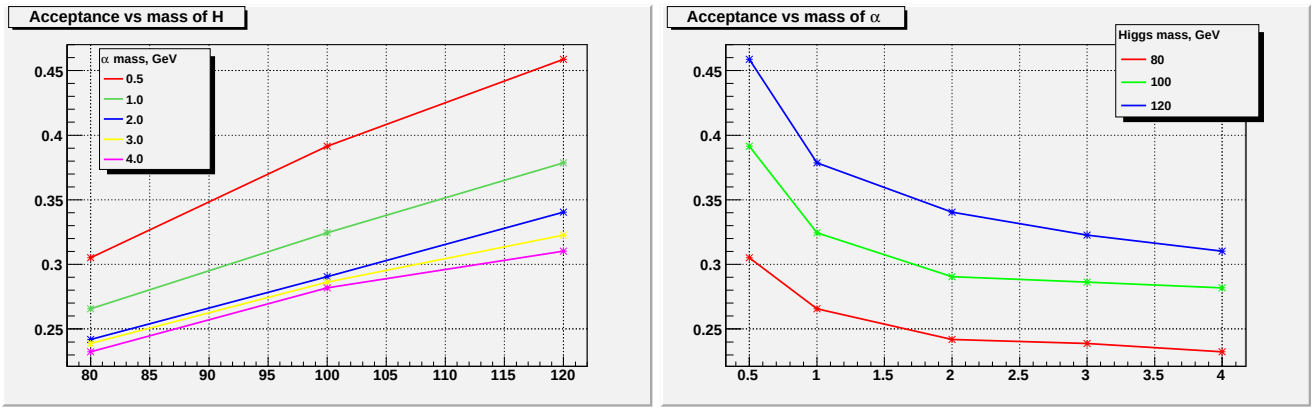

FIG. 6: Acceptance as a function of m_a for fixed m_h. Acceptance as a function of m_h for fixed m_a.

from experimental point of view as the backgrounds will be distributed in some smooth fashion over the 3D space allowing fitting the 3D distribution to estimate backgrounds directly from the data. Potential signal would appear as a concentration of events in one specific region in the 3D space (a 3D "bump"). Figure 7 shows the difference in the reconstructed masses of the two di-muon pairs in signal events, which determines the size of the signal region in the (m_{12}, m_{34}) plane.

To give the reader a better idea on the signal significance of this analysis, we quote efficiencies and background contamination (next section) for a set of cuts that zooms on the highest significance region. The cuts we use are $M > 60$ GeV/c^2, $m_{12} < 4$, $m_{34} < 4$, and $|m_{12} - m_{34}| < 0.08 + 0.005 * (m_{12} + m_{34})$. The latter cut is enforcing the requirement that the two pair masses are consistent with each other and takes into account widening of the absolute resolution in the reconstructed di-muon mass as a function of mass.

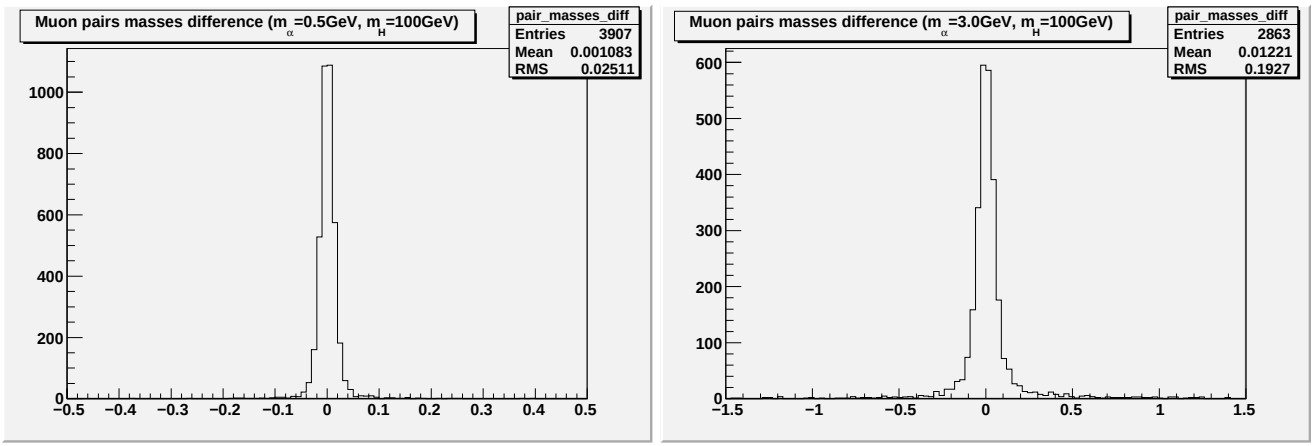

FIG. 7: Left: Muon pairs masses difference (m_a=0.5GeV, m_H=100 GeV). Right: Muon pairs masses difference (m_a=3.0GeV, m_H=100 GeV)

C. Background Estimation

The main backgrounds in this analysis are QCD multijet events where muons originate from either heavy flavor quark decays or from K/π decays in flight. We also considered electroweak backgrounds and direct J/psi production, but found those contributions completely negligible. Requirement of four sufficiently energetic muons in the event drastically reduces contributions of all background processes. Further constarints on the correlation of di-muon pair masses and relatively high invariant mass of the four muon system allows an essentially zero background analysis. In the following we discuss estimation of these backgrounds.

1. QCD backgrounds

The largest contribution comes from rare QCD multi-jet events with four energetic reconstructed muons that are produced either in heavy flavor decays of b and c mesons (real muons) or in K/π decays in flight. The punch-through contamination is heavily suppresed due to massive shileding of the CMS muon system. The multi-jet background is drastically reduced by the requirement of at least one muon with $p_T > 20$ GeV/c and the follow up selections. Background events surviving selections can be divided into two fractions: events with all four real muons from heavy flavor meson decays and events with typically three real muons and a misidentified muon from K/π decays in flight. The first source is estimated using Pythia MC 2→2 QCD jet production by selecting generated muons and smearing distributions using detector resolutions and efficiencies. The second contamination is estimated using the same Pythia sample by selecting events with two or three real muons and one or more charged pions or kaons satisfying p_T and η requirements used for muons. Each such event is assigned a weight calculated as the probability that available K/π mesons decay into muons before reaching radius of $\simeq$2 meters (**halfway into the hadronic calorimeter - is it what we want?**). We find that the level of backgrounds due to misidentifications is comparable to the rate of the backgrounds associated with real muons from heavy flavor decays. While the fraction of remaining events after acceptance cuts does not appear negligible, these events are spread over the 3D space with only a tiny fraction of them appearing in the region where signal would appear, see Tables IV and VI. If necessary, these remaining backgrounds can be completely eliminated by applying a loose track isolation requirement on one of both of the di-muon pairs.

2. Electroweak four lepton backgrounds

We use CompHEP to generate a large sample of events with four muons in final state coming from the electroweak processes. The cross-section of this process is 0.5 pb (Sasha, is this correct? Kind of sounds very small!!!) and after a cut on the first muon $p_T > 20$ GeV/c, the large chunk of remaining events are $Z\gamma^*$ type events. Very few of these events have muons that can be arranged into pairs with low invariant mass, and the fraction of events with similar masses of the pairs is completely negligible.

3. Other SM Backgrounds

We also studied several other processes, e.g. direct J/ψ production process that can produce a pair of muons with mass in the range of interest of this analysis and another pair of muons can come from decays in flight. We used Pythia MC and a weighing technique similar to the QCD case and find that this background is completely negligible. Other SM backgrounds (top, W+jets) are negligible in the region of interest of this analysis.

4. Summary

While the number of background events past the acceptance stage and that are used in the fit is not small, the fitting procedure described in the next section is effectively reducing the region of interest to events that have kinematic properties of signal events making backgrounds nearly completely negligible, as illustarted by the lower part of Table VI showing the number of expected background events after each cut in a dataset corresponding to 100 pb^{-1}of LHC data. **We need a plot to show background distributions, e.g. m12 and m1234 - we have them, just need to clean up**.

IV. STATISTICAL ANALYSIS OF THE DATA

To maximize sensitivity and emulate real data analysis techniques, we define a likelihood function in the 3D space ($m_{pair\ 1},\ m_{pair\ 2}, M$), where M is the four muon invariant mass. The likelihood is defined as follows:

$$\mathcal{L}(m_h, m_a, \sigma(pp{\rightarrow}h)) = \prod_i \mathcal{P}(\sigma(pp{\rightarrow}h)\ L\ BR_{h\rightarrow aa} BR^2_{a\rightarrow\mu\mu} L\alpha(m_h, m_a) N_i^S(m_a, m_h) + L\ N_i^B, N_i^D) \quad (1)$$

where i runs over bins in 3D space of $(m_{12}, m_{34}, m_{1234})$, m_h is the light higgs mass, m_a is axial higgs mass, $\mathcal{P}(\nu, N)$ is Poisson probability for observing N events when the true rate is ν. Other parameters are dataset luminosity L,

TABLE III: Background cuts efficiency for generator level

Cuts	4 leptons	$\mu + x$	J/Ψ
1st eta<2.4	0.7994 ± 0.0040	0.95638 ± 0.00073	0.0088 ± 0.0022
2nd eta<2.4	0.8295 ± 0.0042	0.99992 ± 0.00003	$1.00^{+0.00}_{-0.06}$
3rd eta<2.4	0.8541 ± 0.0044	0.99584 ± 0.00024	0.75 ± 0.11
4th eta<2.4	0.7066 ± 0.0061	0.96407 ± 0.00068	0.75 ± 0.13
1st pt>5	0.9805 ± 0.0022	$1.00000^{+0}_{-0.00001}$	$1.0^{+0.0}_{-0.1}$
2nd pt>5	0.9405 ± 0.0038	0.8676 ± 0.0013	$1.0^{+0.0}_{-0.1}$
3rd pt>5	0.7893 ± 0.0068	0.0445 ± 0.0008	0.3333 ± 0.1571
4th pt>5	0.4390 ± 0.0093	0.0284 ± 0.0032	$0.00^{+0.27}_{-0.00}$
1st pt>20	0.9524 ± 0.0060	0.9873 ± 0.0126	0
analysis acceptance	0.1218 ± 0.0033	0.00099 ± 0.00011	0
pair masses<4	0.0025 ± 0.0014	0.3333 ± 0.0533	0
inv. mass>60	0.6667 ± 0.3333	0.4231 ± 0.0969	0
$\lvert m_{12} - m_{34}\rvert < 0.08GeV + 0.005 * (m_{12} + m_{34})$	$X.XXXX \pm X.XXXX$	$X.XXXX \pm X.XXXX$	0
full efficiency	0.000203 ± 0.000143	0.00014 ± 0.00004	0

TABLE IV: Background cuts efficiency for reco level

Cuts	4 leptons	$\mu + x$	J/Ψ
1st pt>5	0.7455 ± 0.0044	$1.00000^{+0}_{-0.00001}$	$1.0000^{+0}_{-0.0006}$
2nd pt>5	0.7012 ± 0.0053	$1.00000^{+0}_{-0.00001}$	$1.0000^{+0}_{-0.0006}$
3rd pt>5	0.6066 ± 0.0068	0.04349 ± 0.0007	0.3333 ± 0.0013
4th pt>5	0.3300 ± 0.0084	0.0402 ± 0.0034	$0.00^{+0.15}_{-0.00}$
1st pt>20	0.9573 ± 0.0063	$1.000^{+0}_{-0.007}$	0
analysis acceptance	0.1002 ± 0.0030	0.0017 ± 0.0002	0
pair masses<4	0.0041 ± 0.0020	0.3358 ± 0.0403	0
inv. mass>60	0.50 ± 0.25	0.4348 ± 0.0731	0
$\lvert m_{12} - m_{34}\rvert < 0.08GeV + 0.005 * (m_{12} + m_{34})$	$X.XXXX \pm X.XXXX$	$X.XXXX \pm X.XXXX$	0
full efficiency	0.00020 ± 0.00014	0.00025 ± 0.00006	0

acceptance of the signal events $\alpha(m_h, m_a)$, N_i^S is the fraction of reconstructed signal events in bin i ($\Sigma N_i^S = 1$), N_i^B is the rate of background events in bin i per unit of luminosity.

Because of the limited statistics in the Monte Carlo samples describing QCD backgrounds, we parameterize the background distriution in the (m_{12}, m_{34}, M) space using the following function:

$$B(m_{12}, m_{34}, m_{1234}) = f(m_{12}) \times f(m_{34}) \times g(m_{1234}) \quad (2)$$

$$f(m_{12}) = \quad (3)$$

$$g(m_{1234}) =, \quad (4)$$

This simple function describes backgrounds very well in the region of interest because typical four muon invariant mass values are much larger than the narrow range of di-muon pair masses effectively leading to very little correlation of the two. An important note is that using this parameterization requires that in the data analysis the order of pairs has to be randomized (e.g. designating m_{12} to be the mass of the pair that contains highest p_T muon will break factorization), and so we randomize them in the analysis. Fitted parameters of the function are shown in Table **??**. We verified that background events found in MC are well described by this function by running pseudoexperiments using paramaterized distribution and verifying that the p-value for the outcome similar to what is observed in MC is high.

Thus defined likelihood function can be used to calculate the 95% C.L. upper limit on the cross-section times branching ratio of the $h \to \mu\mu\mu\mu$ signal or determine the intergrated luminosity required to make a discovery at a certain level. These results can then be translated into the exclusion region in (m_a, m_h) parameter space or NMSSM parameter space. To demonstrate performance of this technique, Figures 8a) and b) show calculated likelihood functions for two pseudoexperiments, in one of which no signal was injected into the pseudodata and in the other a certain amount of signal was admixed in addition to background contributions. In both cases, likelihood function shows expected behavior.

TABLE V: Expected number of background events after each selection cut on generator level

Cuts	4 leptons	Incl. muon	JPsi
Initial number	48.21 ± 0.49	152878.11 ± 546.06	120.91 ± 2.84
1st eta<2.4	38.54 ± 0.43	146209.61 ± 534.01	1.0652 ± 0.2663
2nd eta<2.4	31.97 ± 0.40	146197.91 ± 533.99	1.0652 ± 0.2663
3rd eta<2.4	27.30 ± 0.37	145589.38 ± 532.88	0.7989 ± 0.2306
4th eta<2.4	19.29 ± 0.31	140358.34 ± 523.22	0.5992 ± 0.1997
1st pt>5	18.92 ± 0.30	140358.34 ± 523.22	0.5992 ± 0.1997
2nd pt>5	17.79 ± 0.30	121774.70 ± 487.35	0.5992 ± 0.1997
3rd pt>5	14.04 ± 0.26	5424.13 ± 102.86	0.1997 ± 0.1153
4th pt>5	6.17 ± 0.17	154.08 ± 17.34	$0^{+0.067}_{-0.000}$
1st pt>20	5.87 ± 0.17	152.13 ± 17.23	$--$
pair masses<4	0.0147 ± 0.0085	50.71 ± 9.95	$--$
inv. mass>60	0.0098 ± 0.0069	21.45 ± 6.47	$--$
$\lvert m_{12} - m_{34}\rvert < 0.08GeV + 0.005 * (m_{12} + m_{34})$	$0.000^{+0.005}_{-0.000}$	$0.00^{+1.95}_{-0.00}$ **??**	$--$

TABLE VI: Expected number of background events after each selection cut on reco level

Cuts	4 leptons	Incl. muon	JPsi
Initial number	48.21 ± 0.49	152878.11 ± 546.06	120.91 ± 2.84
1st pt>5	35.94 ± 0.42	152878.11 ± 546.06	120.91 ± 2.84
2nd pt>5	21.20 ± 0.35	152878.11 ± 546.06	0.3995 ± 0.1631
3rd pt>5	15.29 ± 0.27	6648.99 ± 113.88	$0^{+0.067}_{-0.000}$
4th pt>5	5.04 ± 0.16	267.21 ± 22.83	$--$
1st pt>20	4.83 ± 0.15	267.21 ± 22.83	$--$
pair masses<4	0.0049 ± 0.0098	89.72 ± 13.23	$--$
inv. mass>60	0.0098 ± 0.0069	39.01 ± 8.72	$--$
$\lvert m_{12} - m_{34}\rvert < 0.08GeV + 0.005 * (m_{12} + m_{34})$	$0.000^{+0.005}_{-0.000}$	$0.00^{+1.95}_{-0.00}$ **??**	$--$

We calculate the 95% C.L. upper limit on the product $\sigma(pp\to h)B_{h\to aa}B^2_{a\to\mu\mu}\,\alpha$, using Bayesian technique which is 0.0293 pb at $L = 100$ pb^{-1}, approximately 3 events. In vast majority of pseudoexperiments, this limit is independent of m_h and m_a because the effective signal region that dominates signal significance in the fitter is essentially background free and probability to observe any pseudodata event is very small. Since $B_{a\to\mu\mu}$ is nearly a function of m_a only, it can be factored out, and the corresponding upper limit on $\sigma(pp\to h)B_{h\to aa}\alpha$ is presented in Table VII. The upper limit on $\sigma(pp\to h)B_{h\to aa}$ is shown as a function of m_h and m_a in Table VIII by factoring out α as well. Keep in mind that $B_{h\to aa}$ is close to 100% in much of our preferred region of NMSSM parameter space.

TABLE VII: 95% C.L. on $\sigma(pp\to h)B_{h\to aa}\,\alpha$ at $L = 100$ pb^{-1} as a function of m_a, from Fig 4.

m_a (GeV)	$B_{a\to\mu\mu}$ (%)	$\sigma(pp\to h)B_{h\to aa}\,\alpha$ (pb)
0.5	0	∞
0.75	4.2	16.5
1.0	10.0	2.9
1.5	15.7	1.2
2.0	17.2	1.0
2.5	17.1	1.0
3.0	16.1	1.1
3.5	14.8	1.3
3.75	1.02	282
4.0	0.73	557
5.0	0.49	1220

TABLE VIII: 95% C.L. on $\sigma(pp\to h)B_{h\to aa}$ (pb) at $L = 100$ pb^{-1}, from Fig 4 and Table II.

m_h, m_a (GeV)	0.5	1.0	2.0	3.0	4.0
80	∞	10.9	4.1	4.6	2400
100	∞	8.9	3.4	3.8	2000
120	∞	7.7	2.9	3.4	1800

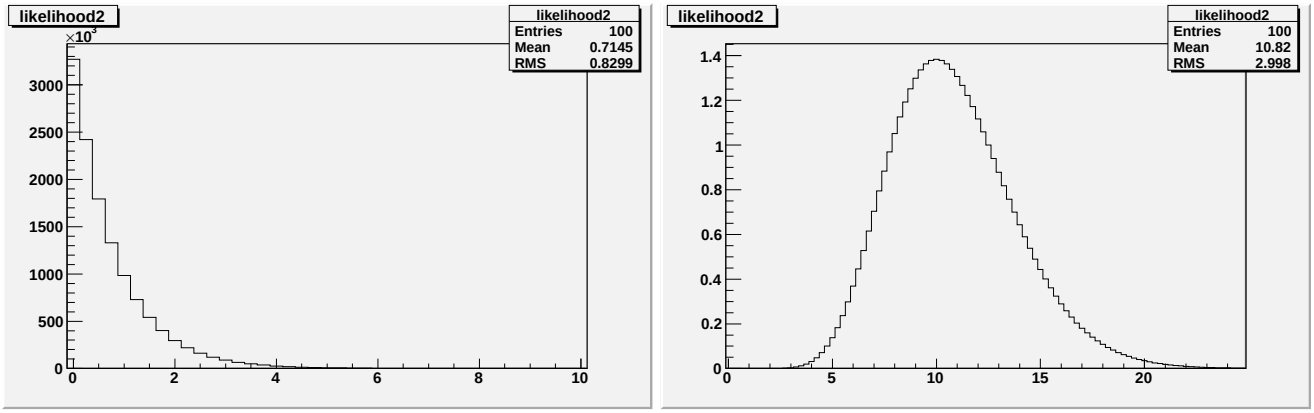

FIG. 8: Left:Example likelihood for a pseudoexperiment for a search assuming $B(H\to aa\to\mu\mu\mu\mu)$=0.04, $m_a = 3$ GeV, $m_h = 100$ GeV with null signal shows that a 95% exclusion is somewhere around 2.5 pb for $\sigma(pp\to H)$. Right: Example likelihood for $\sigma(pp\to H)$=10 pb^{-1}, $B(H\to aa\to\mu\mu\mu\mu)$=0.04, $m_a = 3$ GeV $m_h = 100$ GeV shows a more than 5σ observation.

V. RESULTS

TO BE WRITTEN

Acknowledgments

We thank XXX and YYY

[1] C. Albajar *et al.* (UA1 Collaboration), Phys. Lett. B **253**, 503 (1991); J. Alitti *et al.* (UA2 Collaboration), Phys. Lett. B **276**, 365 (1992).
[2] The LEP Collaborations: ALEPH, DELPHI, L3 and OPAL, the LEP Electroweak Working Group and the SLD Electroweak and Heavy Flavor Working Group (2004), hep-ex/0412015.
[3] T. Affolder *et al.* (CDF Collaboration), Phys. Rev. Lett. **84**, 845 (2000); F. Abe *et al.* (CDF Collaboration), Phys. Rev. D **59**, 052002 (1999); S. Abachi *et al.* (DØ Collaboration), Phys. Rev. Lett. **75**, 1456 (1995); B. Abbot *et al.* (DØ Collaboration), Phys. Rev. D **60**, 053003 (1999).
[4] D. Acosta *et al.* (CDF Collaboration), Phys. Rev. Lett. **94**, 091803 (2005); A. Abulencia *et al.* (CDF Collaboration), FERMILAB-PUB-05-360 (2005), Submitted to Phys. Rev. D.
[5] V.M. Abazov *et al.* (DØ Collaboration), Phys. Rev. D **71**, 072004 (2005).
[6] M. Carena *et al.* , hep-ph/0010338; M. Carena *et al.* , Eur. Phys. J. C **26**, 601 (2003); S. Abel *et al.* , hep-ph/0003154.
[7] S. Belyaev, T. Han, and R. Rosenfeld, JHEP **0307**, 021 (2003).
[8] A. Dedes *et al.* , hep-ph/0207026.
[9] A. Abulencia *et al.* (CDF Collaboration), Phys. Rev. Lett. **96**, 011802 (2006); D. Acosta *et al.* (CDF Collaboration), Phys. Rev. Lett. **95**, 131801 (2005) .
[10] D. Acosta *et al.* (CDF Collaboration), Phys. Rev. D **72**, 072004 (2005).
[11] D. Acosta *et al.* (CDF Collaboration), Phys. Rev. D **71**, 032001 (2005).
[12] S. Baroiant *et al.* , Nucl. Instrum. Methods A **518**, 609 (2004).

TABLE IX: Background samples normalization

Sample	σ	N_{evt}^{gen}	Filter efficiency	L_{eff}	$f = L_{100}/L_{eff}$
$\mu + x$	$0.5091mb$	6238383	0.000239	$51.2709pb^{-1}$	1.9504
4 leptons	$0.538pb$	10995	1.0	$20436.803pb^{-1}$	0.0049
J/ψ	$0.127.2nb$	1413803	0.0074	$1502.00pb^{-1}$	0.0666

[13] S. Klimenko, J. Konigsberg, and T.M. Liss, FERMILAB-FN-0741 (2003).
[14] T. Sjostrand *et al.* , JHEP **0207**, 012 (2002).
[15] J. Pumplin *et al.* , Comput. Phys. Commun. **135**, 238 (2001).
[16] D. Acosta *et al.* (CDF Collaboration), Phys. Rev. Lett. **91**, 241904 (2003).
[17] A. Bhatti *et al.* , Nucl. Instrum. Methods A **566**, 375 (2006).
[18] F. Abe *et al.* (CDF Collaboration), Phys. Rev. D **45**, 1448 (1992).
[19] Particle Data Group, Phys. Lett. B **592**, 1 (2004).
[20] P. Sutton, A. Martin, R. Roberts, and W. Stirling, Phys. Rev. D **45**, 2349 (1992); R. Rijken and W. van Neerven, Phys. Rev. D **51**, 44 (1995); R. Hamberg, W. van Neerven, and T. Matsuura, Nucl. Phys. B **359**, 343 (1991); R. Harlander and W. Kilgore, Phys. Rev. Lett. **88**, 201801 (2002); W. van Neerven and E. Zijstra, Nucl. Phys. B **382**, 11 (1992).
[21] A. Martin, R. Roberts, W. Stirling, and R. S. Thorne, Eur. Phys. J. C **28**, 455 (2003).
[22] R.Brun *et al.* , GEANT Detector Description and Simulation Tool, CERN Program Library, W5013, 1994.
[23] G. Abbiendi *et al.* (OPAL Collaboration), Eur. Phys. J. C **18**, 425-445 (2001).
[24] G. Abbiendi *et al.* (OPAL Collaboration), Eur. Phys. J. C **27**, 483-495 (2003), arXiv:0209068v1 [hep-ex].
[25] U. Ellwanger, J.F. Gunion and C. Hugoine, JHEP **0502**, 066 (2005).
[26] U. Ellwanger, C. Hugoine, Comput. Phys. Commun. **175**, 290 (2006).
[27] F. Domingo and U. Ellwanger, arXiv:0710.3714 [hep-ph].

VI. APPENDIX